

RESEARCH

Open Access



GsMTx4-blocked PIEZO1 channel promotes myogenic differentiation and alleviates myofiber damage in Duchenne muscular dystrophy

Wengang Wang^{1†}, Mingyang Huang^{2†}, Xiusheng Huang^{1†}, Ke Ma³, Ming Luo^{2*} and Ningning Yang^{3*}

Abstract

Background Duchenne muscular dystrophy (DMD) is a debilitating disease characterized by progressive muscle-wasting and a lack of effective therapy. Although the application of GsMTx4 has been shown to reduce muscle mass loss in dystrophic mice, the mechanism of action remains unclear.

Methods We employed single-nucleus RNA sequencing data to scrutinize the expression of mechanosensitive channels in skeletal muscle. The upregulation of PIEZO1 and its precise localization were corroborated in DMD patients, mdx mice, and activated satellite cells. To delve into the role of the GsMTx4-blocked PIEZO1 channel in the myogenic program, we conducted comprehensive in vitro and in vivo studies encompassing the proliferation of satellite cells, differentiation of myoblasts, and calcium influx into myofibers. Utilizing both a PIEZO1 channel inhibitor, GsMTx4, and a PIEZO1 channel agonist, Yoda1, we explored the PIEZO1 channel's impact on satellite cell proliferation and myogenic differentiation. Additionally, we explored the protective effect of the PIEZO1 channel on myofiber calcium influx using mdx mouse models and isolated single myofibers.

Results PIEZO1 was upregulated in the muscle of DMD patients and was predominantly expressed in satellite cells and upregulated during satellite cell proliferation. Treatment with GsMTx4 increased the cross-sectional areas of myofibers and reduced the proportion of centrally nucleated fibers in mdx mice. GsMTx4 inhibited satellite cell proliferation while promoting myogenic differentiation. During myogenic differentiation, the YAP nuclear-cytoplasmic ratio increased in cells treated with GsMTx4 and showed a significant correlation with the nuclear localization of MyoG. In myofibers, GsMTx4 significantly reduced the level of p-CaMKII/CaMKII in muscle and calcium load.

Conclusions PIEZO1 upregulation in DMD could potentially stem from an elevated proportion of proliferating satellite cells triggered by sarcolemma damage and muscle necrosis. The inhibition of the PIEZO1 channel by GsMTx4

[†]Wengang Wang, Mingyang Huang and Xiusheng Huang contributed equally to this work.

*Correspondence:

Ming Luo
luoming1027@whu.edu.cn
Ningning Yang
yangningningzsu@126.com

Full list of author information is available at the end of the article



© The Author(s) 2025. **Open Access** This article is licensed under a Creative Commons Attribution-NonCommercial-NoDerivatives 4.0 International License, which permits any non-commercial use, sharing, distribution and reproduction in any medium or format, as long as you give appropriate credit to the original author(s) and the source, provide a link to the Creative Commons licence, and indicate if you modified the licensed material. You do not have permission under this licence to share adapted material derived from this article or parts of it. The images or other third party material in this article are included in the article's Creative Commons licence, unless indicated otherwise in a credit line to the material. If material is not included in the article's Creative Commons licence and your intended use is not permitted by statutory regulation or exceeds the permitted use, you will need to obtain permission directly from the copyright holder. To view a copy of this licence, visit <http://creativecommons.org/licenses/by-nc-nd/4.0/>.

plays a beneficial role in fostering myogenic differentiation and mitigating myofiber damage. The PIEZO1 channel emerges as a promising therapeutic target for addressing DMD.

Keywords Duchenne muscular dystrophy, PIEZO1, GsMTx4, Satellite cells, Myogenic differentiation

Background

Duchenne muscular dystrophy (DMD) is the first gene-related muscle disease discovered and caused by mutations in the DMD gene encoding dystrophin, a cytoskeletal protein that plays an important role in connecting the cytoskeleton of myofibers with the extracellular matrix [1]. Patients with DMD exhibit progressive muscle degeneration associated with severe muscle weakness, loss of ambulation, and cardiac and respiratory complications [2]. Gene-based therapies are now in various stages of clinical development for DMD, and the most advanced are those targeting the DMD gene using antisense oligonucleotides for exon skipping and CRISPR-based gene editing [3, 4]. In fact, phase III trials with eteplirsen, the FDA-approved morpholino exon-skipping drug, have shown ~1% normal dystrophin levels over 180 weeks, and the disease has thus far defied all curative strategies [5]. Therapeutic methods targeted at enhancing muscle function are extremely important in addition to gene-based technology.

Aberrant calcium regulation contributes to sarcolemmal damage and muscle necrosis in DMD [6].

PIEZO1, a vital mechanosensitive ion channel with a preference for calcium influx, which drives various downstream signaling pathways and governs distinct cellular and physiological responses [7, 8]. Recent studies have illuminated the role of Piezo1 in regulating satellite cell morphology and regenerative capacity under physiological conditions [9]. However, the dual regulatory roles of PIEZO1 in dystrophic muscle—balancing myogenic differentiation and calcium overload—remain unclear. GsMTx4, a peptide derived from spider venom, is recognized for its ability to stabilize lysine residues at the membrane surface, leading to partial relaxation of the outer monolayer and selectively blocking PIEZO1. While GsMTx4 may exhibit partial activity against other channels such as TRPC6 under certain conditions, it is predominantly recognized as the most extensively studied blocker specifically for the PIEZO1 channel [10]. The application of GsMTx4 to dystrophic murine muscle effectively reduces the loss of muscle mass without fibrosis reduction, supporting a model where GsMTx4 acts directly on muscle cells [11]. Similarly, GsMTx4 is reported to be a potent cardioprotectant and to be potentially useful in multidrug strategies to treat ischemia and reperfusion [12]. However, the mechanism of the protective effect of GsMTx4 in muscle remains unclear [13].

In this study, we successfully identified the expression of PIEZO1 in DMD-affected muscle tissue and precisely

determined its localization within the tissue. Moreover, our investigation extensively explored the role of the GsMTx4-blocked PIEZO1 channel in muscle regeneration processes, encompassing satellite cell proliferation, myogenic differentiation, and myofiber calcium dynamics. The opposing effects observed between GsMTx4 and the PIEZO1-specific agonist Yoda1 further corroborate the channel-specific action of GsMTx4 in our experimental models. Our findings underscore that the inhibition of the PIEZO1 channel by GsMTx4 fosters myogenic differentiation through the YAP-MyoG axis and attenuates myofiber damage by reducing the calcium load. These results strongly suggest that targeting the PIEZO1 channel holds significant promise as a therapeutic strategy for treating DMD.

Methods

Human muscle samples and the GEO database

Following approval from the Ethics Committee and obtaining informed consent from each patient's guardian, we procured muscle tissue samples from DMD patients aged 5 to 10 years, and muscle tissue from a control group of age-matched males who had undergone orthopedic surgery. The detailed information of the DMD patients was presented in supplementary Table 1. Subsequently, the collected tissue samples were bifurcated: one portion was promptly frozen in pre-cooled isopentane for immunohistochemistry, and the other portion was rapidly frozen in liquid nitrogen for subsequent RNA-seq, quantitative polymerase chain reaction (qPCR), and Western blot assays.

To validate the variance in gene expression, we retrieved RNA-seq data (GSE6011 and GSE38417) from the GEO database and conducted a comparative analysis of PIEZO1 expression between DMD patients and controls. All single-nucleus RNA sequencing data were directly sourced from the GEO database. Petrony et al. utilized snRNA-seq to determine the extent of transcriptional diversity within multinucleated skeletal myofibers and based on this normal mouse skeletal muscle sequencing data, we examined the expression levels of *Piezo1* in different cell types (GSE147127). Chemello et al. described the creation of a mouse model of DMD caused by deletion of exon 51 of the dystrophin gene, which represents a prevalent disease-causing mutation in humans. Using their snRNA-seq data, we analyzed the compositional differences of different cell types in skeletal muscle between mdx mice and wild-type mice (GSE156498). The methodologies for single-nucleus RNA

sequencing of skeletal myofibers and its application in the context of muscular dystrophy were previously elucidated by Petrany et al. and Chemello et al., respectively [14, 15].

Acute muscle injury model and Mdx mice

Following approval from the Ethics Committee, C57BL/6 mice were procured from Dossy Experimental Animals Co., Ltd., and 8-week-old mice were specifically chosen for in vivo exploration of myogenic capability. To induce an acute muscle injury model, 50 μ l of cardiotoxin (CTX) at a concentration of 10 μ M (Latoxan, #L8102) were intramuscularly injected into the tibialis anterior (TA) muscle, utilizing a 31 G insulin syringe. For the mdx mouse model, we used the C57BL/6Smoc-Dmd^{em1(Q995X)Smoc} strain, which typically exhibits muscle fiber necrosis starting at 4–7 weeks of age, and consistently shows muscle phenotypes resembling clinical DMD by 3 months of age. All mice used in the study were male. To evaluate the therapeutic effect of GsMTx4, we initiated drug intervention in 3-month-old mice. After phenotypic validation, 3-month-old mdx mice were selected to assess the therapeutic efficacy of the PIEZO1 channel blocker in vivo. The stock solution of Yoda1 (AbMole, #M9372) was prepared at a concentration of 10mM in DMSO, resulting in a DMSO concentration of 1:2000 in the working solution. GsMTx4 (MCE, #HY-P1410) was dissolved in PBS and prepared at a concentration of 10mM. Intramuscular injections of 50 μ l of GsMTx4 (5 μ M) or Yoda1 (5 μ M) were administered to the TA muscle of the right hindlimb using a 31 G insulin syringe, with PBS serving as the vehicle control.

EdU incorporation was visualized using the BeyoClick™ EdU-488 kit (Beyotime #C0071S) according to the manufacturer's protocol. Briefly, EdU was dissolved in drinking water at a concentration of 0.3 mg/mL, and the solution was freshly prepared daily. EdU administration commenced on day 7 post-CTX injury and continued until sample collection on day 21 post-CTX injury. Grip strength was assessed using a grip strength meter (SA417, Sansbio). The mdx mice were gently held by the tail and lowered toward the grid until both hindlimbs grasped it. The tail was pulled horizontally until the mouse released its grip, and the peak force was recorded. Five trials were conducted per mouse, with a 1-minute rest interval between trials. The average of the three highest values was used for analysis to minimize variability. The TA muscles were harvested and measured for further use.

Satellite cells and single myofibers

Satellite cell cultures were established using four-week-old mice, and satellite cells were extracted following established protocols [16]. These cells were maintained under controlled conditions of 37 °C and 5% CO₂. The

expression of Piezo1 was assessed using immunofluorescence and qPCR at various intervals to track changes during satellite cell activation. To elucidate the role of the PIEZO1 channel in these cells, we incubated them with GsMTx4 (5 μ M) and Yoda1 (5 μ M), followed by immunofluorescence analysis and cell counts after a 3-day incubation. Additionally, Piezo1 expression in proliferating satellite cells was compared between wild-type (WT) and mdx mice using Western blot assays.

Isolation of single myofibers was conducted from the extensor digitorum longus (EDL) muscle. The EDL muscles were subjected to prewarmed collagenase solution and placed in a 37 °C water bath for 60 min to facilitate myofiber release. Subsequently, single myofibers were mechanically dissociated by triturating with Pasteur pipettes of decreasing bore size. Myofibers were also isolated from 3-month-old mdx mice. Fluo-4 AM (Beyotime, #S1060) served as a fluorescent indicator for measuring calcium influx. Loading with Fluo-4 AM (5 μ M) was performed for 20 min, followed by perfusion with Hank's Balanced Salt Solution for an additional 30 min. Treatment with Yoda1 (5 μ M) and GsMTx4 (5 μ M) was conducted for 10 min, and Fluo-4 AM signals were continuously collected over 30 min, following the experimental protocol. Fluo-4 AM fluorescence was captured using a fluorescence microscope (ECLIPSE Ti2, Nikon, Japan) with 488 nm illumination. Background subtraction was applied, and relative calcium intensity was calculated as $(F - F_0)/F_0$, where F represents fluorescence and F₀ indicates basal fluorescence levels.

Primary cell derived myoblasts culture and myogenic differentiation

We obtained myoblasts from primary satellite cells. These cells were cultured under standard conditions at 37 °C with 5% CO₂ and expanded through subculturing in growth medium containing 20% fetal bovine serum (Gibco). Upon reaching a cell density of 90%, the culture medium was replaced with differential medium containing 2% horse serum (Hyclone). All siRNAs targeting *Piezo1* were custom-designed and synthesized by RIBOBIO. The transfection of siRNAs into cells was accomplished using Lipofectamine™ RNAiMAX Reagent (Invitrogen, #13778150) following the manufacturer's instructions. The efficiency of *Piezo1* knockdown was validated through Western blot analysis. Additionally, GsMTx4 (5 μ M) and Yoda1 (5 μ M and 10 μ M) were introduced into the differential medium, and the expression levels of genes associated with myogenic differentiation were assessed using both qPCR and immunofluorescence techniques.

Immunohistochemistry and Immunofluorescence

Human muscle samples and mouse TA muscle tissues were cryopreserved in isopentane pre-cooled with liquid nitrogen. Subsequent slicing was executed using a refrigerated slicing machine (Leica, Germany) with a thickness of 8 mm, followed by fixation in 4% paraformaldehyde for 20 min. Haematoxylin and eosin (H&E) staining procedures were conducted according to the manufacturer's guidelines. Muscle tissue sections underwent a blocking step with 10% goat serum for 2 h, followed by permeabilization with 1% Triton X-100 for 20 min. Cultured cells were fixed in 4% paraformaldehyde for 20 min, subjected to a 2-hour blocking with 10% goat serum, and permeabilized with 1% Triton X-100. For immunohistochemistry, the PIEZO1 primary antibody (1:200, Proteintech, #15939-1-AP) was incubated with the samples overnight at 4 °C. DAB was employed for restaining and film sealing. In the case of immunofluorescence, tissue sections and cells were incubated with primary antibodies against PIEZO1 (1:200, Proteintech, #15939-1-AP), PAX7 (1:5, DSHB, #PAX7), Ki67 (1:200, Proteintech, #27309-1-AP), MHC (1:10, DSHB, #MF20), and MyoG (1:50, DSHB, #F5D) at 4 °C overnight. Subsequently, a fluorescence secondary antibody (Goat Anti-Rabbit/Mouse IgG H&L, Abcam, Alex Fluor 488/594) was applied at room temperature for 2 h. The specificity of the PIEZO1 antibody for immunofluorescence used in this study was verified with siRNA-mediated knockdown experiments. Images were acquired after DAPI staining, utilizing a fluorescence microscope (ECLIPSE Ti2, Nikon, Japan) or a laser scanning confocal microscope (STELLARIS 5, Leica, Germany).

The complete section of the TA muscle was assessed for each replicate. Utilizing Image J software (Version 1.52v), the cross-sectional area of myofibers and proportion of centrally nucleated fibers were quantified from stained sections. The fibrotic area, corresponding to the area stained in red, was measured based on five individual microscope fields. Hematoxylin stains the nuclei blue, and eosin stains the cytoplasm pink, allowing for clear visualization of both the nuclei and muscle fiber structure. The centrally nucleated fibers were identified based on the position of the nucleus in relation to the fiber in the analyzed field. Specifically, differentiated myotubes were identified by their staining with MHC, a marker indicative of mature myotubes, while MHC-negative cells were indicative of undifferentiated myoblasts. The fusion index was calculated by determining the ratio of myonuclei within myotubes to the total number of nuclei. A myotube was defined as having at least two nuclei within the same cytoplasm. The widest segment of the muscle fiber cross-section was chosen as the measurement for myotube width. In total, five fields from a minimum of

three distinct replicate samples were analyzed for this assessment.

qPCR and Western blot assay

Tissue or cell lysates were prepared using TRIzol, and subsequent total RNA extraction followed the prescribed protocols provided by the manufacturer. Following RNA isolation, the concentration and purity of the RNA were assessed. For reverse transcription, 1 µg of total RNA was employed. Quantitative PCR (qPCR) analysis was conducted utilizing the SYBR method (Vazyme, #Q111-02), employing primer sequences specified in the [Supplementary Tables](#). Relative expression levels of target genes were determined using the $2^{-\Delta\Delta CT}$ method. The qPCR reactions were performed using the QuantStudio 3 instrument. (Thermo Fisher Scientific, USA).

Total protein extraction was carried out using RIPA lysis buffer supplemented with 1% PMSF, and protein quantification was conducted using the BCA method. Cytosolic and membrane fractions were isolated using the Mem-PER Plus Membrane Protein Extraction Kit (Thermo Fisher Scientific, #89842). In brief, muscle tissue underwent washing with a wash buffer and subsequent division into small pieces. Permeabilization buffer was added, and constant mixing ensued until achieving a homogeneous suspension. Centrifugation at $16,000 \times g$ for 15 min resulted in the pelletization of permeabilized cells, and the supernatant containing cytosolic proteins was collected. The pellet was then resuspended in solubilization buffer, subjected to centrifugation, and the supernatant containing membrane-associated proteins was collected for future use.

Following standard electrophoresis and membrane transfer protocols, membranes were blocked with 5% BSA. Overnight incubation at 4 °C followed with primary antibodies against PIEZO1 (1:1000, Proteintech, #15939-1-AP), Dystrophin (1:500, Santa Cruz, #sc-365954), and p-CaMKII (1:200, Santa Cruz, #sc-32289). Subsequently, membranes were incubated with the secondary antibody (HRP-conjugated Affinipure Goat Anti-Rabbit/Mouse IgG, Proteintech, #SA00001-1 and #SA00001-2) for 2 h at room temperature. Signal detection was performed using a Chemiluminescent Imaging System (BioRad, USA). Grayscale values of the target protein were analyzed using Image J software (Version 1.52v) to calculate the relative expression level, with a minimum of three independent sample repetitions.

Statistical analysis

Statistical analysis was conducted using GraphPad Prism (Version 8.4.3). Continuous variables were presented as mean \pm SD, and a normality test was executed. Student's t-test was employed to compare continuous variables between two groups, whereas one-way ANOVA was

utilized for multi-group comparisons. The parameter 'n' denoted an independent biological sample, and each sample's measurement was derived from an average of three technical replicates. A *P* value less than 0.05 was deemed statistically significant.

Results

Upregulated PIEZO1 in skeletal muscle of DMD

We investigated the expression of mechanosensitive calcium channels in healthy skeletal muscle, with a specific focus on the transient receptor potential channel and PIEZO channel families. Utilizing RNA-seq data for channel screening, we compared the expression levels of mechanosensitive calcium channels between normal and DMD muscles, revealing the up-regulation of TRPC1 and PIEZO1 in DMD patients (Fig. 1A). To further substantiate these findings, we validated the results using two GEO datasets (Fig. 1B-C). Additionally, we confirmed the increased expression of PIEZO1 in DMD patient samples through qPCR and Western blot assays (Fig. 1D-F). Collectively, these results provide evidence supporting the upregulation of PIEZO1 in the skeletal muscle of individuals with DMD.

Upregulated PIEZO1 in DMD results from proliferating satellite cells

To explore the potential selective expression of *Piezo1* within specific cell types, we assessed *Piezo1* expression

across diverse cell populations using single-nucleus sequencing data for skeletal muscle. Our findings reveal predominant expression of *Piezo1* in satellite cells, endothelial cells, and tenocytes (Fig. 2A). Previous reports have indicated an increased satellite cell count in DMD subsequent to muscle damage [17]. Immunofluorescence staining of muscle tissue was conducted to determine the localization of the Piezo1 protein. Strong positive signals of Piezo1 were detected surrounding myofibers and beneath the sarcolemma, co-localizing with Pax7 (Fig. 2B). Further verification of Piezo1 preferential expression in proliferating satellite cells was accomplished using plated satellite cells and single myofiber model (Fig. 2C-D). To delineate the relationship between PIEZO1 and satellite cell activation, satellite cells were isolated from uninjured muscle of wild-type mice and cultured for 2 days under proliferative conditions. After two days of plated culture, qPCR analysis of satellite cells demonstrated synchronized upregulation of *Piezo1* alongside the marker genes for satellite cells, *Pax7* and *MyoD* (Fig. 2E). These collective findings indicate the preferential expression of *Piezo1* in proliferating satellite cells.

To discern the primary cause of the heightened PIEZO1 expression in DMD, we conducted a comparative analysis of satellite cell proportions in healthy and DMD patients. Our findings indicate an increased proportion of PAX7⁺ cells and PIEZO1⁺/PAX7⁺ cells in

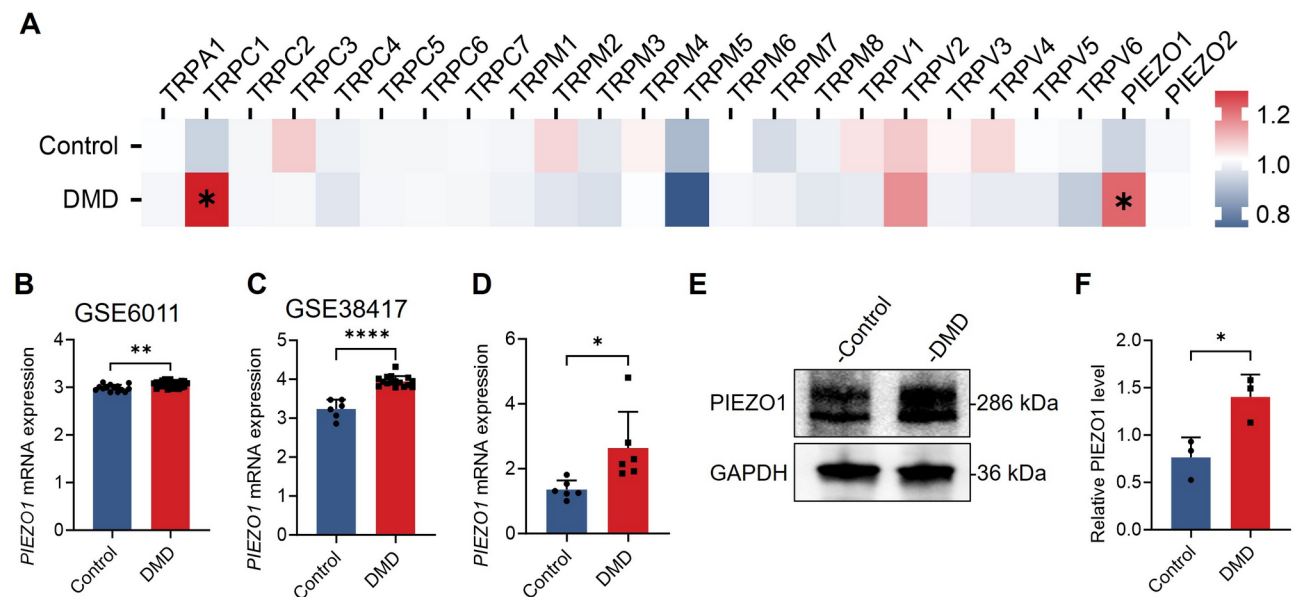


Fig. 1 Upregulated PIEZO1 in skeletal muscle of DMD patients. **(A)** The expression of mechanosensitive calcium channels, including members of the transient receptor potential channel family and Piezo channel family ($n=5$; mean; Student's *t*-test). **(B)** The expression of *PIEZO1* was upregulated in muscle tissue of DMD patients according to GEO datasets GSE6011 ($n=14\sim 23$; mean \pm SD; Student's *t*-test). **(C)** The expression of *PIEZO1* was upregulated in muscle tissue of DMD patients according to GEO datasets GSE38417 ($n=6\sim 16$; mean \pm SD; Student's *t*-test). **(D)** The expression of *PIEZO1* was upregulated in the muscle tissue of DMD patients according to qPCR ($n=6$; mean \pm SD; Student's *t*-test). **(E-F)** Representative Western blot of PIEZO1 in muscle tissue of DMD patients, and the relative PIEZO1 level was significantly increased in DMD patients ($n=3$; mean \pm SD; Student's *t*-test). Statistical significance was set at $P < 0.05$. * $P < 0.05$; ** $P < 0.01$; **** $P < 0.0001$

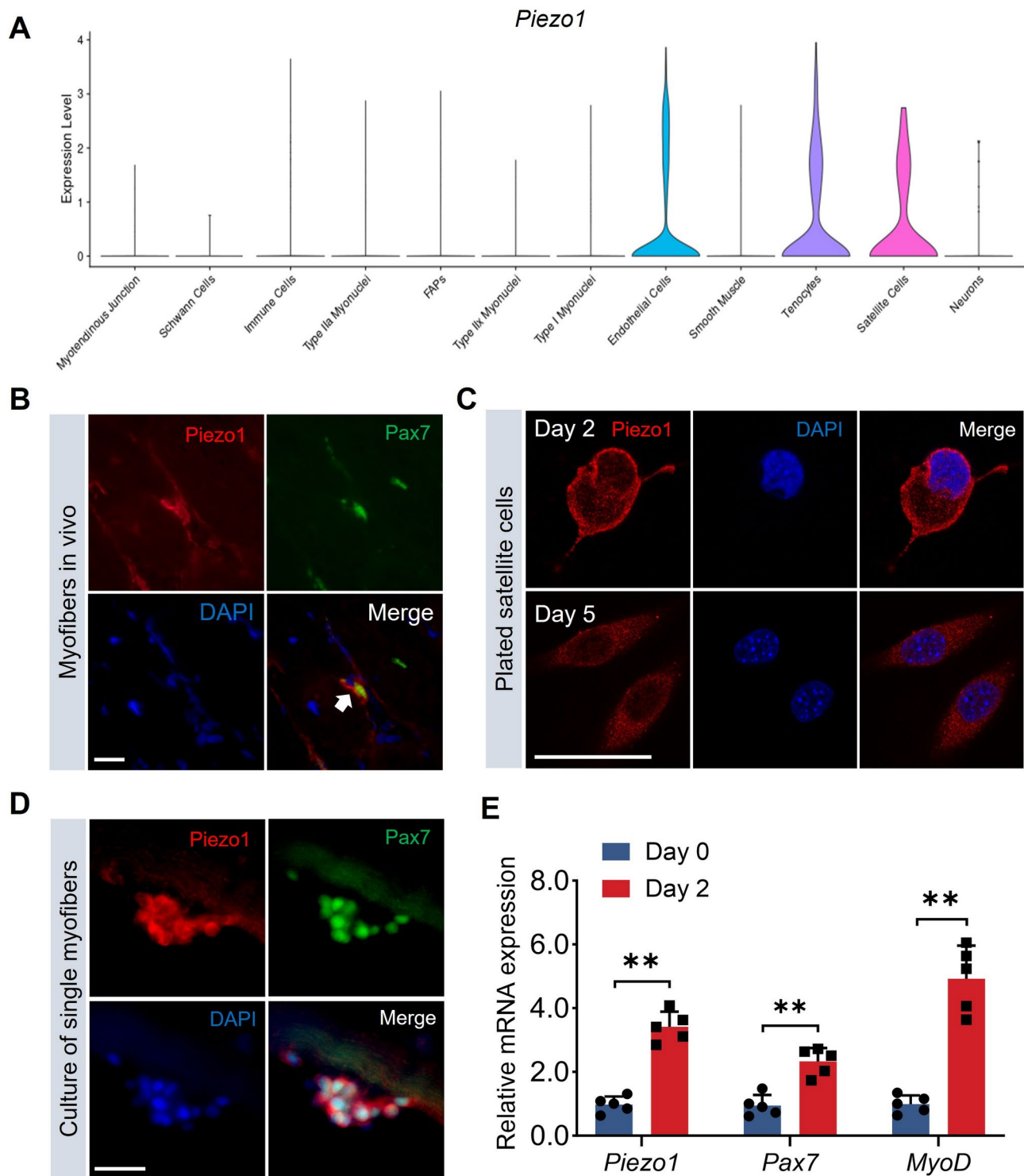


Fig. 2 PIEZO1 is preferentially expressed in activated satellite cells. **(A)** The expression pattern of *Piezo1* in different subsets of cells in skeletal muscle according to single-nucleus RNA sequencing dataset showed that *Piezo1* was predominantly highly expressed in satellite cells, endothelial cells, and tenocytes. **(B)** Immunofluorescence colocalization analysis showed that *Piezo1* was preferentially expressed on the cell membrane of satellite cells in vivo. **(C)** Immunofluorescence colocalization analysis showed that *Piezo1* was preferentially expressed on the cell membrane of satellite cells in plated satellite cells. **(D)** Immunofluorescence colocalization analysis showed that *Piezo1* was preferentially expressed on the cell membrane of satellite cells of single myofiber. **(E)** qPCR showed that the mRNA expression of *Piezo1*, *Pax7*, and *MyoD* were upregulated in muscle tissue after CTX injection ($n=5$; mean \pm SD; Student's t-test). Statistical significance was set at $^{**}P < 0.01$. Scale bar, 50 μ m

DMD patients (Fig. 3A-C). Previous findings reveal predominant expression of *Piezo1* in satellite cells, endothelial cells, and tenocytes (Fig. 2A), we therefore assessed the composition of distinct cell types in mdx mice using single-nucleus sequencing data. The results revealed an elevation in the proportion of proliferating satellite cells in mdx mice (6.6% vs. 5.3%), accompanied by a significant reduction in endothelial cell proportion (3.4% vs. 8.6%), with no alteration in the proportion of tenocytes (2.5% vs. 2.5%) (Fig. 3D). To eliminate the possibility of pathological expression intrinsic to satellite cells, we isolated satellite cells from both WT and mdx mice and extracted total protein. However, Western blot analysis failed to discern any differences in *Piezo1* relative expression (Fig. 3E-F). Immunofluorescence staining of muscle tissue revealed a moderate fluorescent signal on the sarcolemma, yet no significant differences were observed in the intensity of *Piezo1* on the sarcolemma between WT and mdx mice (Fig. 3G-H). Collectively, these results suggest that the elevated PIEZO1 expression in DMD may arise from the increased presence of proliferating satellite cells, which are activated in response to muscle necrosis.

GsMTx4-blocked PIEZO1 channel ameliorates muscular dystrophy in mdx mice

To assess the potential of the PIEZO1 channel as a therapeutic target for DMD treatment, we initially characterized the muscular dystrophy phenotype through Western blot assays (Fig. 4A). Subsequently, we administered GsMTx4 (5 μ M) and Yoda1 (5 μ M) injections into the TA muscles of mdx mice over a 30-day period (Fig. 4B). H&E staining revealed notable outcomes following GsMTx4 treatment, including an increase in the cross-sectional area of myofibers and a reduction in the proportion of centrally nucleated fibers (Fig. 4C-E), additional functional assessments also showed an increased grip strength (Fig. 4F). Conversely, activation of the PIEZO1 channel by Yoda1 led to decreased myofiber cross-sectional area and grip strength (Fig. 4G-J). Moreover, after a 30-day treatment with GsMTx4, H&E staining of vital organs such as the heart, liver, spleen, lung, and kidney, and no obvious tissue toxicity of GsMTx4 was observed in mdx mice (Fig. S1). These findings suggest that inhibiting the PIEZO1 channel with GsMTx4 holds promise in alleviating muscular dystrophy in mdx mice.

GsMTx4-blocked PIEZO1 channel inhibits satellite cell proliferation while promoting myogenic differentiation

We further explored the impact of the GsMTx4-blocked PIEZO1 channel on satellite cell proliferation and myogenic differentiation. For satellite cell proliferation assessment, plated satellite cells were treated with GsMTx4 (5 μ M) and Yoda1 (5 μ M) for a period of 3 days. Notably, GsMTx4 treatment significantly reduced the percentage

of Ki67⁺ cells and the total cell count, while Yoda1 treatment exhibited a stimulatory effect on satellite cell proliferation (Fig. 5A-C). These findings indicate that the GsMTx4-blocked PIEZO1 channel hinders satellite cell proliferation.

Piezo1 expression was observed to be downregulated during satellite cell differentiation into myoblasts (Fig. 5D), implying that *Piezo1* downregulation may facilitate the transition from proliferation to differentiation. Yoda1 (5 μ M and 10 μ M) was introduced to myoblasts cells during the transition from complete to differentiated medium at a cell density of 90%, strategically mitigating the confounding effects of cell proliferation. We found that Yoda1 treatment impeded myogenic differentiation in a concentration-dependent manner (Fig. 5E-H). Conversely, siRNA knockdown of *Piezo1* in myoblasts resulted in an elevation of the fusion index, and Yoda1 treatment partially prevented the uncontrolled fusion of myotubes (Fig. S2A-E). Subsequently, we delved into the potential role of the GsMTx4-blocked PIEZO1 channel in myogenic differentiation. GsMTx4 (5 μ M) was introduced to myoblasts during the transition from complete to differentiated medium at a cell density of 90%. Cells treated with GsMTx4 exhibited a pronounced increase in the fusion index, MyoG-positive nuclei index, and myotube width (Fig. S2G-J). These outcomes suggest that the GsMTx4-blocked PIEZO1 channel promotes myogenic differentiation in vitro.

We further investigated the potential of the GsMTx4-blocked PIEZO1 channel to promote myogenic differentiation in vivo. Satellite cells typically exit the cell cycle and undergo differentiation into myotubes approximately 5 days after CTX-induced muscle injury [18]. To minimize any potential confounding effects of GsMTx4 treatment on satellite cell proliferation, we administered GsMTx4 (5 μ M) and Yoda1 (5 μ M) five days after inducing muscle injury with CTX, and the muscles were subsequently stained (Fig. 6A). Our findings indicate that GsMTx4 treatment resulted in an increased TA muscle weight and cross-sectional area of myofibers, a reduction in the proportion of centrally nucleated fibers, the expression of *Pax7*, and the proportion of PAX7⁺ cells. These changes collectively suggest enhanced myogenic differentiation (Fig. 6B-H). In contrast, Yoda1 treatment led to a decrease in TA muscle weight and cross-sectional areas, the expression of *Pax7* and *Piezo1*, and the proportion of PAX7⁺ cells, implying a delay in the regeneration process (Fig. 6B-H). We further identified newly incorporated myonuclei within regenerating myofibers via EdU staining. Our results demonstrated that GsMTx4 treatment for 2 weeks significantly increased the proportion of peripheral EdU-positive cells beneath the sarcolemma, but no central EdU⁺ nuclei were observed within the fiber. This suggests that GsMTx4 promotes myoblast

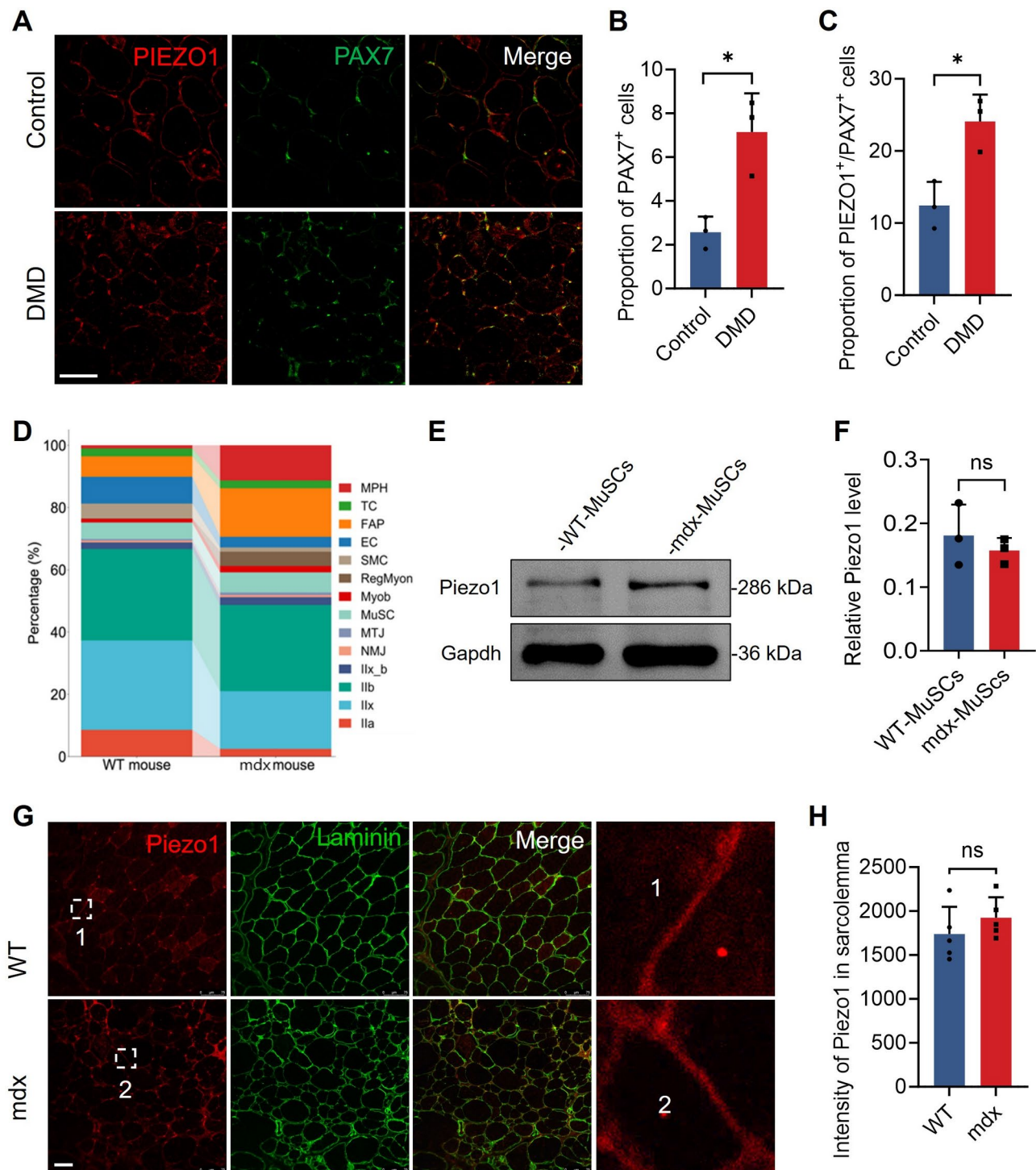


Fig. 3 Upregulated PIEZO1 results from proliferating satellite cells. **(A-C)** Representative immunofluorescence images showed increased proportion of PAX7⁺ cells and PIEZO1⁺/PAX7⁺ cells in the muscle tissue of DMD patients ($n=3$; mean \pm SD; Student's *t*-test). **(D)** The proportions of different cell types in the tibialis anterior muscles of WT and mdx mice. **(E-F)** Representative Western blot of Piezo1 in satellite cells of WT and mdx mice, and no significant changes in the relative Piezo1 level in WT and mdx mice. ($n=3$; mean \pm SD; Student's *t*-test). **(G-H)** Representative immunofluorescence images showed that Piezo1 was expressed in the sarcolemma and some specific cells, and no significant changes in the intensity of Piezo1 in sarcolemma ($n=5$; mean \pm SD; Student's *t*-test). Ilia indicates type Ila myonuclei; Ilx, type Ilx myonuclei; Ilb, type Ilb myonuclei; Ilx_b, type Ilx_b myonuclei; NMJ, neuromuscular junction myonuclei; MTJ, myotendinous junction myonuclei; MuSC, muscle satellite cells; Myob, myoblasts; RegMyon, regenerative myonuclei; SMC, smooth muscle cells; EC, endothelial cells; FAP, fibro/adipogenic progenitors; TC, tenocytes; MPH, macrophages. Statistical significance was set at $P < 0.05$. * $P < 0.05$. Scale bar, 50 μ m

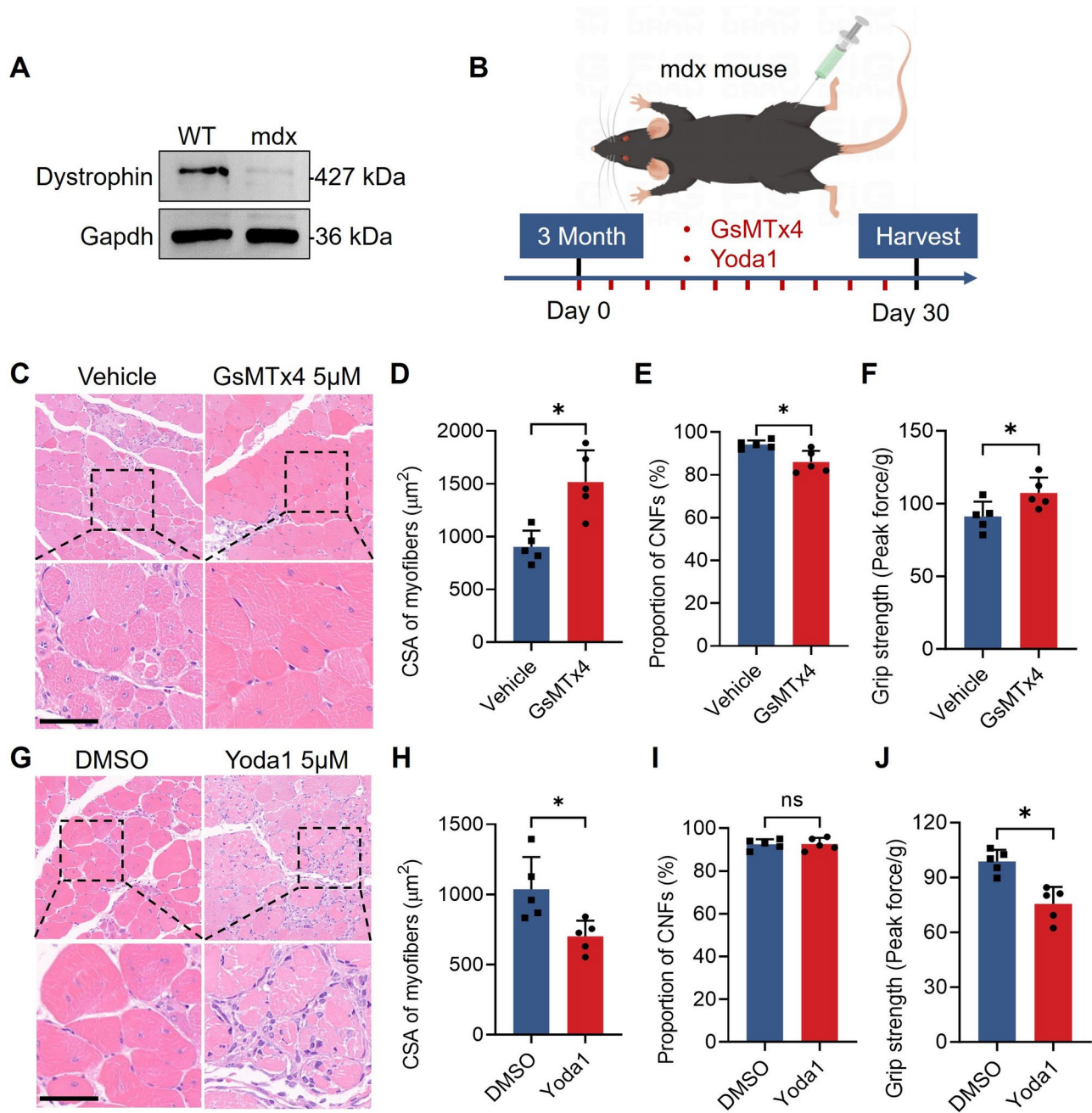


Fig. 4 GsMTx4-blocked PIEZO1 channel ameliorates muscular dystrophy in mdx mice. **(A)** Representative Western blot of dystrophin in muscle tissue of WT and mdx mice. **(B)** Flow diagram of the treatment in mdx mice, the red markings indicate the time points for drug injections. **(C)** Representative H&E images show myofibers treated with GsMTx4 for 30 days. **(D-F)** The cross-sectional area of myofibers and grip strength were increased, and the proportion of centrally nucleated fibers was decreased after treatment with GsMTx4 ($n=5$; mean \pm SD; Student's t -test). **(G)** Representative H&E images show myofibers treated with Yoda1 for 30 days. **(H-J)** The cross-sectional area of myofibers and grip strength were decreased after treatment with Yoda1 ($n=5$; mean \pm SD; Student's t -test). Statistical significance was set at $P < 0.05$. * $P < 0.05$. Scale bar, 50 μ m

fusion at the investigated time points (Fig. S3A-C). These results strongly suggest that the GsMTx4-blocked PIEZO1 channel has the potential to promote myogenic differentiation in vivo.

Mechanically, we investigated the impact of blocking or activating the PIEZO1 channel on the nucleocytoplasmic

distribution of YAP during myogenic differentiation. Interestingly, we found that the total YAP N/C ratio increased in cells treated with GsMTx4 (5 μ M), while it decreased when treated with Yoda1 (Fig. 7A-B). XMU-MP-1, a specific inhibitor of MST1/2, partially rescued the nuclear aggregation of YAP, along with the expression

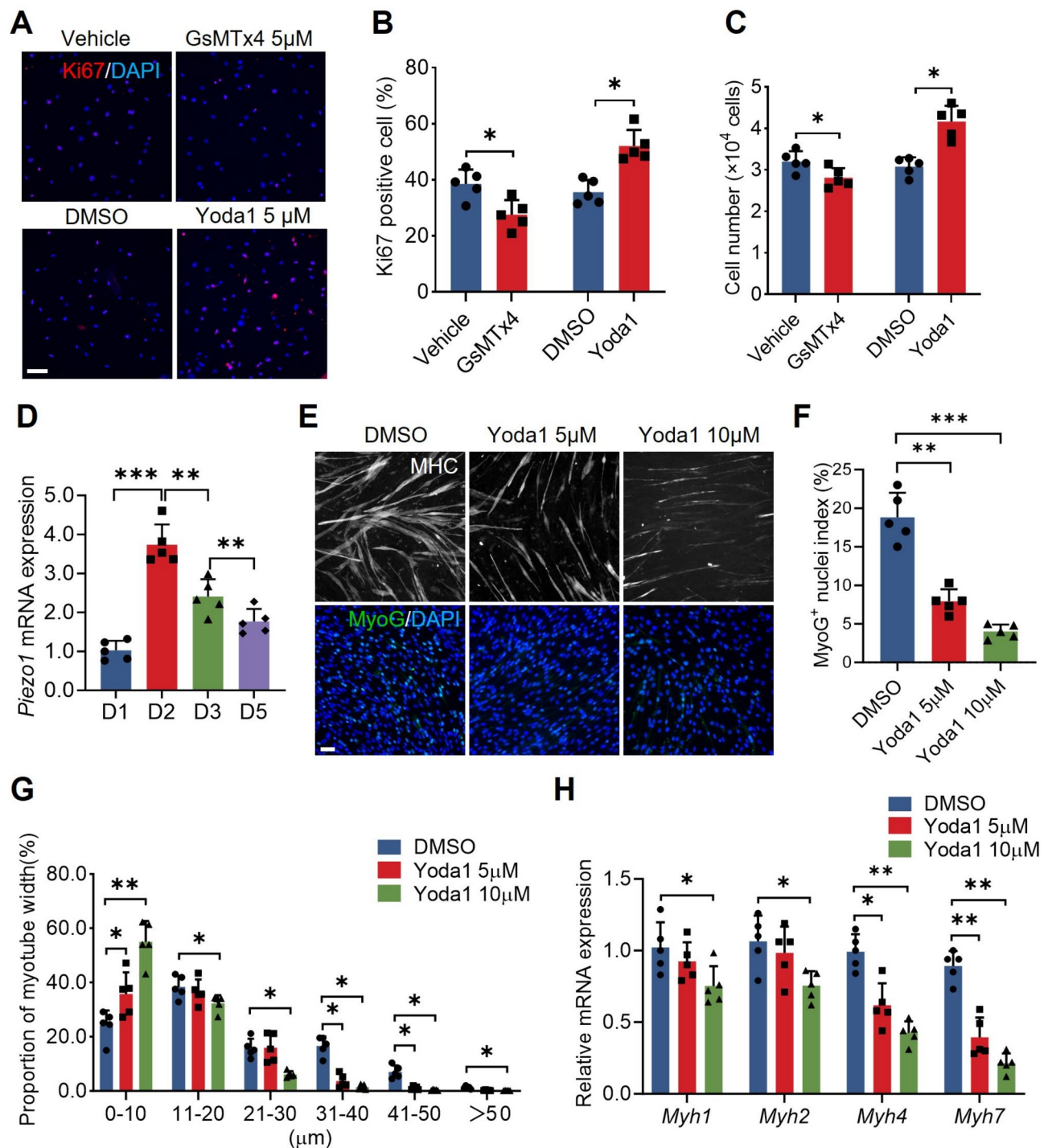


Fig. 5 Activating PIEZO1 channel inhibits myogenic differentiation in vitro. **(A)** Representative immunofluorescence images of Ki67 for GsMTx4 treatment satellite cells. **(B)** GsMTx4 treatment decreased the percentage of Ki67-positive cells, and Yoda1 treatment increased the percentage of Ki67-positive cells ($n=5$; mean \pm SD; Student's t-test). **(C)** Cell counts analysis showed consistent trends with the immunofluorescence analysis of Ki67 ($n=5$; mean \pm SD; Student's t-test). **(D)** qPCR analysis showed that *Piezo1* was upregulated in plated satellite cells at Day 2 and declined gradually at Day 5 ($n=5$; mean \pm SD; One-way ANOVA). **(E)** Representative immunofluorescence images showed that Yoda1 treatment restrained myogenic differentiation in a concentration-dependent manner. **(F)** The MyoG positive nuclei index was decreased after treatment with Yoda1 ($n=5$; mean \pm SD; One-way ANOVA). **(G)** The myotube width were decreased after treatment with Yoda1 ($n=5$; mean \pm SD; One-way ANOVA). **(H)** qPCR showed that the expression levels of *Myh1*, *Myh2*, *Myh4* and *Myh7* were decreased after treatment with Yoda1 ($n=5$; mean \pm SD; One-way ANOVA). Statistical significance was set at $P < 0.05$. * $P < 0.05$; ** $P < 0.01$; *** $P < 0.001$. Scale bar, 50 µm

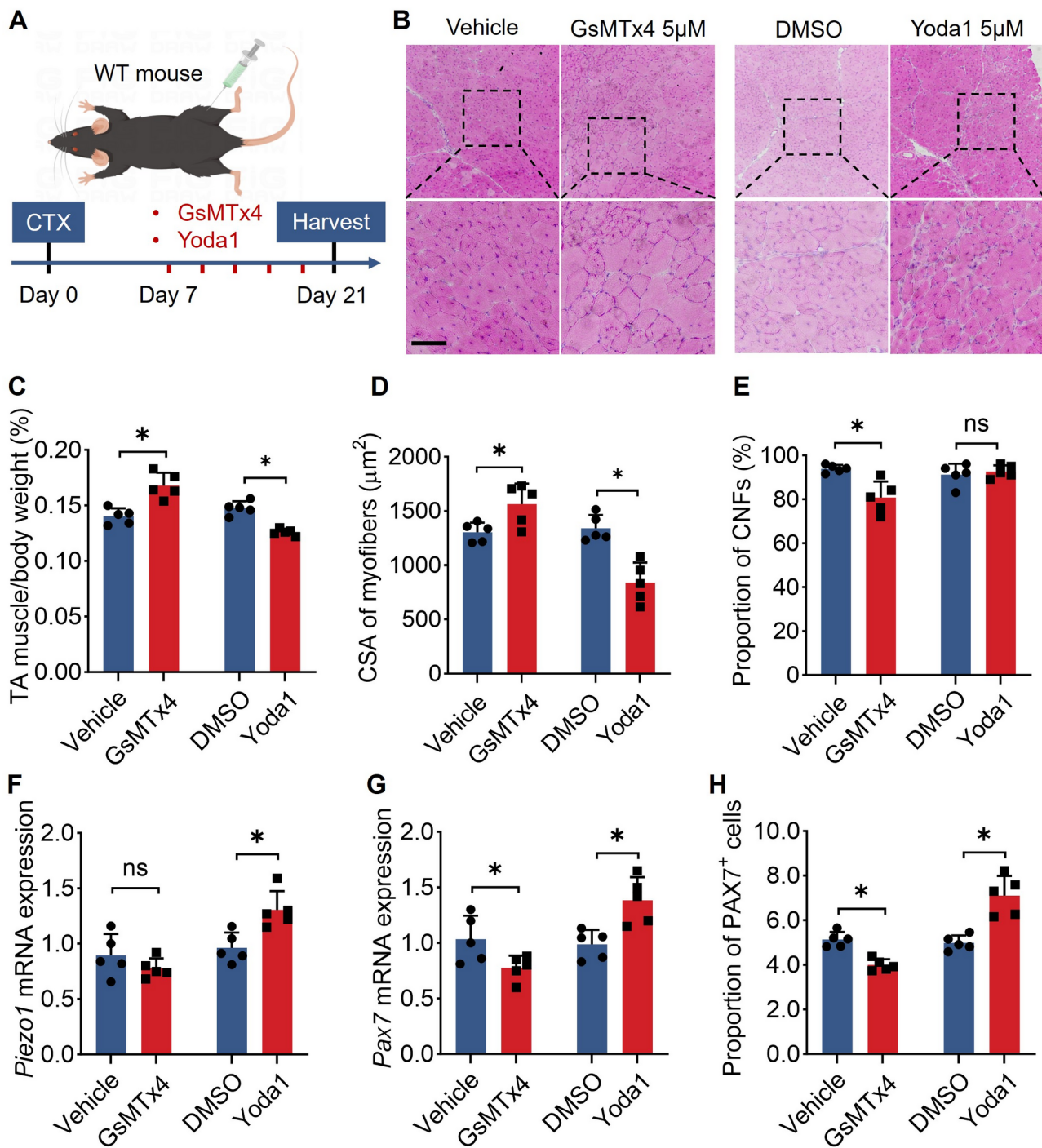


Fig. 6 GsMTx4-blocked PIEZO1 channel promotes myogenic differentiation in vivo. **(A)** Flow diagram of the experiment in WT mice, the red markings indicate the time points for drug injections. **(B)** Representative H&E images show myofibers treated with GsMTx4 and Yoda1. **(C)** The weight of tibialis anterior muscle was increased after treatment with GsMTx4 and decreased after treatment with Yoda1 ($n=5$; mean \pm SD; Student's t-test). **(D)** The cross-sectional area of myofibers was increased after treatment with GsMTx4 and decreased after treatment with Yoda1 ($n=5$; mean \pm SD; Student's t-test). **(E)** The proportion of centrally nucleated fibers was decreased after treatment with GsMTx4 ($n=5$; mean \pm SD; Student's t-test). **(F)** *Piezo1* expression was increased after treatment with Yoda1 ($n=5$; mean \pm SD; Student's t-test). **(G)** *Pax7* expression was decreased after treatment with GsMTx4 and increased after treatment with Yoda1 ($n=5$; mean \pm SD; Student's t-test). **(H)** The proportion of PAX7⁺ cells was increased after treatment with Yoda1 ($n=5$; mean \pm SD; Student's t-test). Statistical significance was set at $P < 0.05$. * $P < 0.05$; ** $P < 0.01$. Scale bar, 50 µm

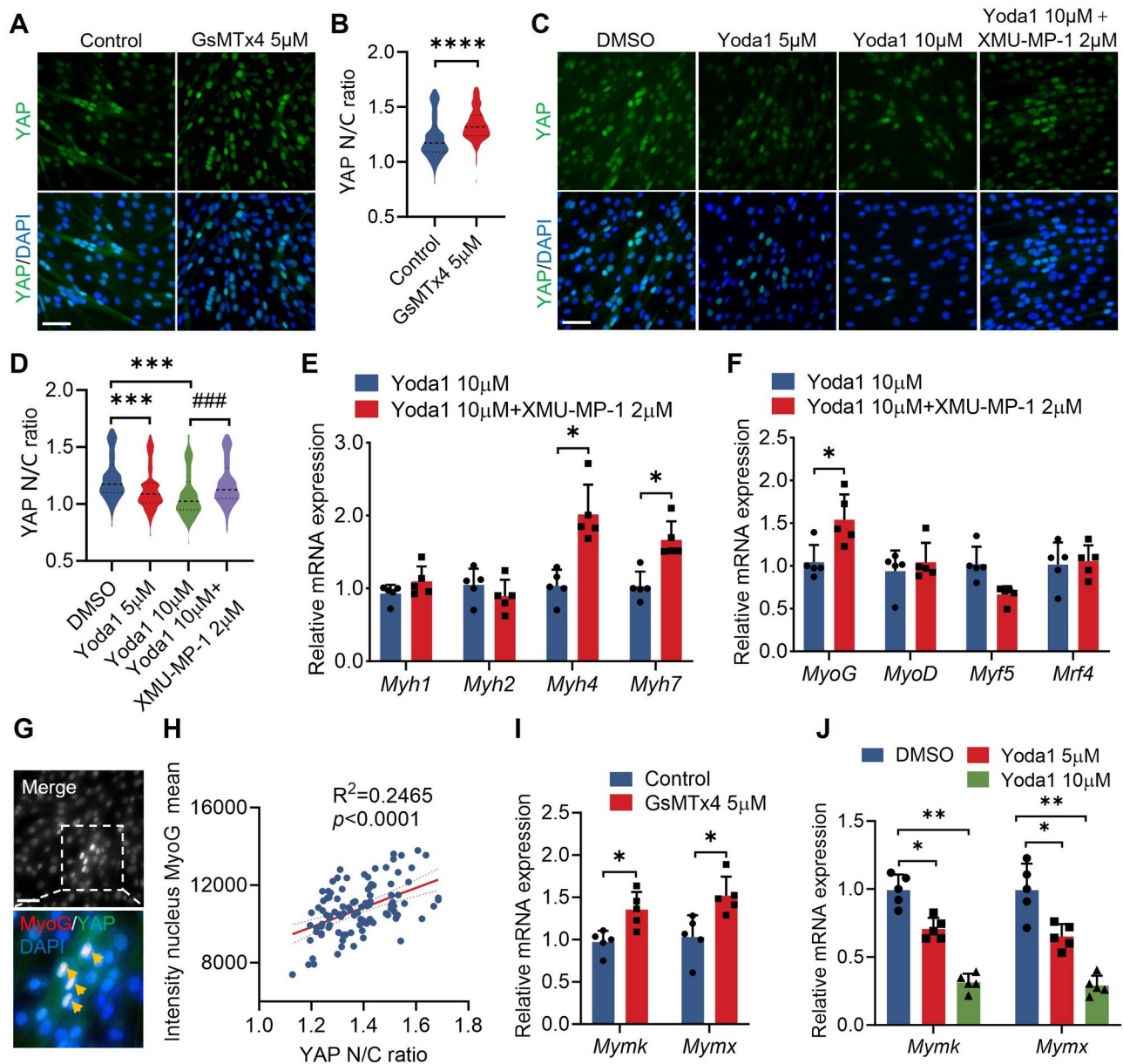


Fig. 7 GsMTx4-blocked PIEZO1 channel promotes myogenic differentiation through YAP-MyoG axis. **(A)** Representative immunofluorescence images of YAP after myogenic differentiation after treatment with GsMTx4 for 3 days. **(B)** The YAP N/C ratio was increased after treatment with GsMTx4 ($n = 114 \sim 145$; mean; Student's t-test). **(C)** Representative immunofluorescence images of YAP after myogenic differentiation after treatment with Yoda1 for 3 days. **(D)** The YAP N/C ratio was decreased after treatment with Yoda1, and XMU-MP-1 partially rescued the suppressive effect of Yoda1 on YAP N/C ratio ($n = 85 \sim 109$; mean; One-way ANOVA). **(E)** XMU-MP-1 treatment partially rescued the suppressive effect of Yoda1 on *Myh4* and *Myh7* expression ($n = 5$; mean \pm SD; Student's t-test). **(F)** XMU-MP-1 treatment partially rescued the suppressive effect of Yoda1 on *MyoG* expression ($n = 5$; mean \pm SD; Student's t-test). **(G)** Immunofluorescence colocalization analysis showed that YAP and MyoG were aggregated in the nuclei of the differentiated myotubes. **(H)** Correlation analysis showed that the YAP N/C ratio was positively correlated with the mean intensity of the MyoG nucleus ($n = 107$; Pearson correlation coefficient method). **(I)** *Mymk* and *Mymx* expression were increased after treatment with GsMTx4 ($n = 5$; mean \pm SD; Student's t-test). **(J)** *Mymk* and *Mymx* expression were decreased after treatment with Yoda1 ($n = 5$; mean \pm SD; Student's t-test). Statistical significance was set at $P < 0.05$. * $P < 0.05$; ** $P < 0.01$; *** $P < 0.001$; **** $P < 0.0001$; ### $P < 0.001$. Scale bar, 50 μ m

of *Myh4* and *Myh7* (Fig. 7C-D). Furthermore, we investigated the expression of myogenic regulatory factors, including *MyoG*, *MyoD*, *Myf5*, and *Mrf4*. The qPCR results showed a significant increase in *MyoG* expression after treatment with XMU-MP-1 (Fig. 7E-F). The

immunofluorescence revealed the colocalization of YAP and MyoG in myotubes, and Pearson correlation analysis showed a significant correlation between YAP N/C and the mean intensity of nuclear MyoG (Fig. 7G-H). Finally, we found that the expression of *Mymk* and *Mymx*,

downstream targets of *MyoG*, was significantly increased after treatment with GsMTx4. Conversely, Yoda1 treatment inhibited the expression of *Mymk* and *Mymx* in a concentration-dependent manner (Fig. 7I-J). Taken together, these results suggest that GsMTx4-blocked PIEZO1 channel promotes myogenic differentiation through the YAP-MyoG axis.

GsMTx4-blocked PIEZO1 channel inhibits calcium overload in myofibers

The absence of dystrophin stands as a pivotal pathological hallmark in DMD, leading to heightened membrane permeability, facilitating calcium influx, and subsequent myofiber damage [19]. In our pursuit to pinpoint the localization of the Piezo1 protein, we conducted immunofluorescence staining of muscle tissue from mdx mice, revealing a moderate fluorescent signal predominantly localized on the sarcolemma (Fig. 8A). While this aligns with the established notion that PIEZO1 is a mechanically sensitive ion channel residing on the cell membrane's surface, it's crucial to note that its expression on the sarcolemma was comparatively less pronounced

than that observed in satellite cells. The sustained escalation of calcium influx through surface-bound PIEZO1 channels can induce diverse phenotypic alterations in the skeletal muscles of mdx mice owing to the activation of calcium-dependent enzymes. Supporting this premise, the relative level of p-CaMKII/CaMKII was notably elevated in mdx skeletal muscle following treatment with Yoda1. Conversely, the relative level of p-CaMKII/CaMKII significantly decreased post-treatment with GsMTx4 (Fig. 8B-C), indicating a reduction in calcium load within myofibers in vivo. To delve deeper into GsMTx4's potential to impede calcium entry in individual myofibers, we isolated single myofibers from the EDL muscle and quantified calcium influx using the fluorescent indicator Fluo-4 AM. Following a 10-minute treatment with GsMTx4 (5 μ M), a substantial restriction in relative calcium influx was evident, whereas incubation with Yoda1 (5 μ M) led to increased calcium influx (Fig. 8D-G). Collectively, these in vivo and in vitro findings strongly suggest that GsMTx4, a PIEZO1 channel inhibitor, attenuates calcium overload in myofibers by suppressing mechanosensitive calcium influx.

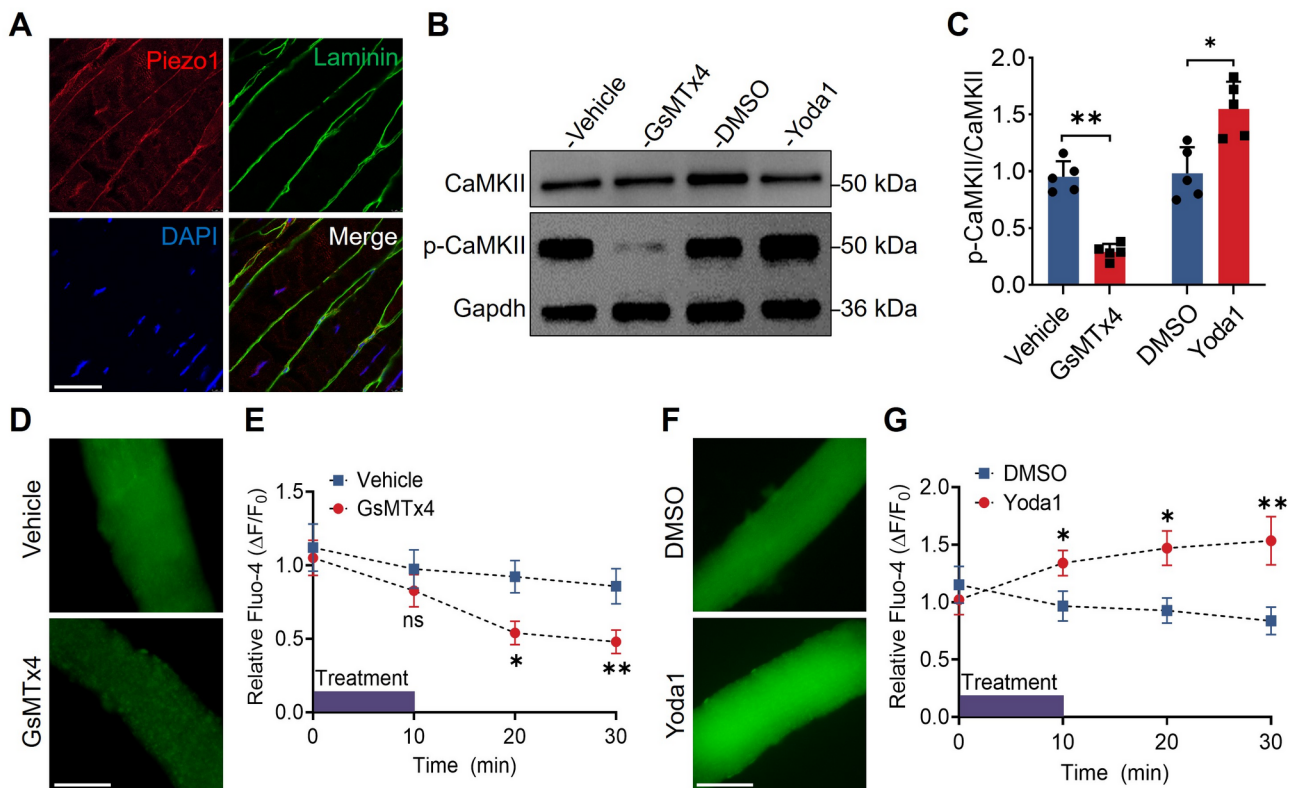


Fig. 8 GsMTx4-blocked PIEZO1 channel inhibits calcium overload in myofibers of mdx mice. **(A)** Representative immunohistochemical images showed that Piezo1 was expressed in the sarcolemma of mdx mice. **(B-C)** Representative Western blot of CaMKII and p-CaMKII after treatment with GsMTx4 and Yoda1 in mdx mice, and the relative p-CaMKII/CaMKII level was significantly increased decreased after treatment with GsMTx4 and increased after treatment with Yoda1 in mdx mice ($n=5$; mean \pm SD; Student's t-test). **(D)** Representative immunohistochemical images after treatment with GsMTx4. **(E)** The relative calcium influx in isolated single myofiber was significantly restrained after treatment with GsMTx4 ($n=5$; mean \pm SD; One-way ANOVA). **(F)** Representative immunohistochemical images after treatment with Yoda1. **(G)** The relative calcium influx in isolated single myofiber was significantly increased after Yoda1 was added ($n=5$; mean \pm SD; One-way ANOVA). Statistical significance was set at $P < 0.05$. * $P < 0.05$. Scale bar, 50 μ m

Table 1 Recent studies on the role of Piezo1 in skeletal muscle

Authors	Function	Main conclusion
Hirano et al. [21]	Satellite cell regeneration	PIEZO1 promotes proliferation and regenerative functions of MuSCs through precise control of cell division.
Ma et al. [9]	Morphologies of satellite cell	Satellite cells were classified into three functionally distinct stem cell states: responsive, intermediate, and sensory. Yoda1 treatment promoted an increased percentage of responsive satellite cells.
Quiroga et al. [22]	Myogenic differentiation	Short-term treatment with Yoda1 significantly enhanced cell fusion
Peng et al. [23]	Satellite cell activation	Piezo1 represses activation, leading to fewer satellite cell via cell senescence.
Hirata et al. [34]	Muscle atrophy	Acute disruption of Piezo1 in skeletal muscle induced Klf15 and Il6 expression as well as muscle atrophy.

Discussion

The current study reveals an upregulation of PIEZO1 in the skeletal muscles of individuals with DMD, with a preferential expression observed in satellite cells. Moreover, our findings offer compelling evidence that the inhibition of the PIEZO1 channel, achieved through GsMTx4, effectively restrains the proliferation of satellite cells, fosters myogenic differentiation, and provides a protective effect against myofiber damage induced by calcium influx. The targeted inhibition of the PIEZO1 channel emerges as a promising therapeutic strategy for DMD, offering the potential to enhance myogenic differentiation while mitigating calcium overload in myofibers.

Using the GEO databases, clinical muscle samples, muscle injury model, and satellite cells culture method, we screened several mechanosensitive channels and identified that PIEZO1 was upregulated in DMD. Recently, Scripture-Adams et al. developed a methodology to efficiently isolate individual nuclei from minute quantities of frozen skeletal muscle [20]. They performed single-cell distribution analysis on WT and mdx mice, and the results were similar to those of our single-cell data analysis, with a significant increase in satellite cells in mdx mice (4.28% vs. 2.23%) but a decrease in endothelial cells (7.48% vs. 14.73%). They further analyzed the activation status of satellite cells and found that all of them were quiescent in WT mouse (2.23%), while mdx mice had proportions of quiescent, early activated, and late activated cells at 2.42%, 1.43%, and 0.44%, respectively [20]. This indicates that the increased number of satellite cells in mdx mice is mainly composed of proliferating satellite cells, especially early activated ones. Our study found that *Piezo1* expression was significantly upregulated in the activation phase of satellite cells, and the proportion of PIEZO1⁺/PAX7⁺ cells was significantly increased in DMD, further supporting the view that the increased PIEZO1 expression in DMD is due to the proliferating satellite cells.

Our results suggest that GsMTx4-blocked PIEZO1 channel suppresses the proliferation of satellite cells. Hirano et al. employed a genetic engineering approach in mice, which demonstrated that *Piezo1*-deficient satellite cells exhibit proliferation defects via Rho-GTPase

signalling, ultimately affecting cytokinesis [21]. Our findings complement but critically extend the work of Ma et al., who highlighted *Piezo1*'s role in satellite cell responsiveness during physiological regeneration [9]. While their study elegantly linked *Piezo1* to cytoskeletal remodeling in healthy muscle, we uncover its pathological duality in DMD: PIEZO1 upregulation drives aberrant satellite cell proliferation while exacerbating calcium-mediated myofiber damage. The therapeutic inhibition of PIEZO1 thus achieves a dual benefit—restoring differentiation capacity and mitigating necrosis—that is uniquely relevant to dystrophic pathology. This distinction underscores the importance of context-specific PIEZO1 modulation, as its roles in healthy versus dystrophic muscle are mechanistically and therapeutically divergent. We summarised the recent studies on the role of PIEZO1 in skeletal muscle (Table 1).

In contrast to inhibiting satellite cell proliferation, the GsMTx4-blocked PIEZO1 channel promotes myogenic differentiation. However, a previous study reported that short-term treatment with Yoda1 significantly enhanced cell fusion [22]. The different drug treatment regimens could be one of the reasons that explain the contrasting results. In Quiroga's study, short-term treatments (within 1 h) of Yoda1 promoted myogenic differentiation, and they admitted that continued activation (4 h) showed a significant decrease in the fusion of myotubes. In our study, Yoda1 was added to the differential medium for 3 days. In the *Piezo1* loss-of-function study, Quiroga et al. reported that the knockdown of *Piezo1* in early-formed myotubes confirmed a significant reduction in the fusion index [22]. Another recent study reported that *Piezo1*^{scKO} myoblasts were reduced by approximately 50% compared to the control [23]. Interestingly, Quiroga et al. also admitted their contrasting results with another study, which reported that *Piezo1* deficiency promoted myoblast fusion [24]. Recently, academic perspectives on the PIEZO1 channel, such as the "Time Window" effect [25], cortical actomyosin assembly [24], force-from-filament model [8], and mechano-transduction complex [26], have been proposed. The function of PIEZO1 may be far more complex and intricate than a simple ion channel on the cell surface as initially thought.

Most satellite cells reacquire quiescence 5–10 days post-muscle injury, following the differentiation and fusion of the majority of cells to regenerate myofibers [27]. To further investigate how PIEZO1 modulates the temporal dynamics of myonuclear incorporation, we employed EdU labeling and discovered that GsMTx4-mediated blockade of PIEZO1 channels elevated the proportion of EdU-positive cells beneath the sarcolemma, indicative of myocyte-myofiber fusion. These findings align with recent perspectives suggesting that early-phase density-dependent myocyte fusion, occurring within residual basement membrane tubes of necrotic myofibers, whereas late-phase myocyte-myofiber fusion contributes to their radial expansion [28]. Mechanistically, prior work has identified YAP as a novel regulator of C2C12 myogenesis [29]. Importantly, our data revealed that PIEZO1 inhibition via GsMTx4 enhanced nuclear localization of YAP and upregulated the expression of fusion-associated genes (MyoG, Mymk, and Mymx), thereby extending these regulatory dynamics to the mechanosensitive PIEZO1 pathway.

Previous studies have provided evidence that stretch-activated channels are an important source of calcium influx [30–33]. PIEZO1, a vital mechanosensitive ion channel with a preference for calcium influx, can be blocked by GsMTx4 and selectively activated by Yoda1 [13]. In this study, the proportion of centrally nucleated fibers and the phosphorylated CaMKII in mdx muscles, and the calcium load in single myofibers were decreased after treatment with GsMTx4. These results suggest that the GsMTx4-blocked PIEZO1 channel exerts some protection against myofiber calcium overload. Hirata et al. reported a role for the Piezo1/KLF15/IL-6 axis in immobility-induced muscle atrophy, and that the CaMK pathway acts as Piezo1's downstream effector in muscle [34]. There are a few potential explanations for these differing conclusions. First, the roles of CaMKK and CaMKII in skeletal muscle are not mutually exclusive but rather exhibit considerable overlap. They are more likely to function in a downstream-upstream relationship: CaMKK is an upstream kinase that regulates signaling pathways by activating other downstream kinases, such as AMPK and CaMKII [35]. Furthermore, the experimental conditions in the two studies may vary in ways that influence PIEZO1 signaling. For instance, Hirata et al. focused on chronic muscle mass maintenance, while our study explored acute effects of Piezo1 activation in the context of dystrophic muscle. The mdx mouse model, which we used, has distinct characteristics compared to the healthy muscles studied by Hirata et al., which may also explain the differential responses observed in terms of muscle mass regulation and signaling pathways [34].

Many mechanosensitive ion channels have been reported to regulate calcium entry in myofibers. PIEZO1

is activated by mechanical stimuli, and it is responsible for an inward current induced by mechanical stimulation in C2C12 myotubes [34]. TRPV2 was localized in the sarcolemma of mdx fibers, and specific inhibition of TRPV2 led to a significant amelioration of muscle pathology by inhibiting calcium entry in myofibers [36]. The expression of TRPC1 is increased in mdx muscle, and it might contribute to the elevated calcium load in myofibers, which is characteristic of muscular dystrophy [37]. Overexpression of TRPC3 and the associated increase in calcium influx resulted in a phenotype of muscular dystrophy, and inhibition of TRPC channels in mice dramatically reduced calcium influx in myofibers and dystrophic disease manifestations [38]. TRPC6 contributed to abnormal calcium stress responses in cardiomyocytes from mice lacking dystrophin, and pharmacological TRPC6 inhibition improved muscle function in mdx mice [32]. Recent studies have largely solidified the calcium hypothesis of muscular dystrophy, such that models with artificially elevated calcium in skeletal muscle manifest fulminant dystrophic-like disease, whereas models with enhanced calcium clearance or inhibited calcium influx are resistant to myofiber death and muscular dystrophy [33]. Hirata et al. reported a role for the Piezo1/KLF15/IL-6 axis in immobility-induced muscle atrophy, which uncovered an important role of Piezo1 in regulating cytosolic calcium concentration [34]. Therefore, we propose that the GsMTx4-blocked PIEZO1 channel exerts some protection against myofiber damage in mdx mice by inhibiting calcium influx. These findings are expected to provide new ideas for the treatment of DMD and related muscle damage diseases.

This study possesses several limitations. Firstly, GsMTx4 may influence PIEZO1 function in satellite cells, thereby altering the delicate balance between proliferation and differentiation, the benefits of this shift in either direction for tissues exhibiting discordant satellite cell states and ongoing regeneration remain unclear. Further investigation is warranted to elucidate the intricate regulatory role of PIEZO1 in the maturation process of muscles. Secondly, there is currently no small molecule drug available for the specific inhibition of the PIEZO1 ion channel. To enhance the credibility of our results, we introduced Yoda1, a specific activator of the PIEZO1 channel, for comparison. The observed opposing effects compared to GsMTx4 reinforce our conviction that GsMTx4 exerts a crucial role through the PIEZO1 ion channel. Thirdly, while our findings strongly support the therapeutic potential of PIEZO1 modulation in DMD, we acknowledge that the absence of genetic validation (e.g., *Piezo1*-conditional knockout in mdx mice) limits mechanistic certainty. Future studies employing such models are essential to confirm the satellite cell-autonomous versus systemic roles of PIEZO1 in dystrophic pathology.

Nevertheless, our complementary pharmacological and molecular approaches—combined with human tissue validation—provide robust preliminary evidence to justify further exploration.

Conclusion

PIEZO1 exhibits upregulation in the skeletal muscle of individuals with DMD, with preferential expression observed in satellite cells. The heightened expression of PIEZO1 in DMD is posited to emanate from the proliferating satellite cells. Blocking the PIEZO1 channel with GsMTx4 has demonstrated the ability to impede the proliferation of satellite cells, facilitate myogenic differentiation, and provide protection against myofiber damage induced by calcium influx. The PIEZO1 channel, identified through these findings, holds promise as a prospective therapeutic target for addressing the challenges associated with DMD.

Abbreviations

DMD	Duchenne muscular dystrophy
qPCR	Quantitative polymerase chain reaction
CTX	Cardiotoxin
TA	Tibialis anterior
WT	Wild-type
EDL	Extensor digitorum longus
H&E	Haematoxylin and eosin

Supplementary Information

The online version contains supplementary material available at <https://doi.org/10.1186/s13395-025-00383-5>.

Supplemental Table 1: Detailed information of the Duchenne muscular dystrophy patients

Supplemental Table 2: Real-time quantitative PCR primers designed for human samples

Supplemental Table 3: Real-time quantitative PCR primers designed for mouse samples

Supplemental materials: The full-size Western blot images

Supplementary Figure 1: Representative H&E images of heart, liver, spleen, lung, and kidney after treating with GsMTx4 for 30 days. Scale bar, 50µm

Supplementary Figure 2: GsMTx4-blocked PIEZO1 channel promotes myogenic differentiation in vitro. **(A-B)** Representative Western blot of *Piezo1* knockdown in primary cell derived myoblasts for 3 days. The relative *Piezo1* level was significantly decreased ($n=3$; mean \pm SD; Student's *t*-test). **(C-D)** Representative immunofluorescence images of MHC for *Piezo1* knockdown primary cell derived myoblasts cells after myogenic differentiation for 3 days, and the fusion index was significantly increased in *Piezo1* knockdown myoblasts and partly rescued by Yoda1 treatment ($n=5$; mean \pm SD; Student's *t*-test). **(E-H)** Representative immunofluorescence images showed that GsMTx4 treatment promoted myogenic differentiation, and the fusion index and myogenin positive nuclei index, and myotube width were increased after treatment with GsMTx4 ($n=5$; mean \pm SD; Student's *t*-test). **(I)** qPCR showed that the expression levels of *Myh4* and *Myh7* were upregulated after treatment with GsMTx4 ($n=5$; mean \pm SD; Student's *t*-test). Statistical significance was set at $P < 0.05$. * $P < 0.05$; ** $P < 0.01$. Scale bar, 50µm

Supplementary Figure 3: EdU labeling and administration in vivo. **(A)** Schematic diagram of the experimental timeline in WT mice. Red markings indicate time points for drug injections, while green arrows denote the administration of EdU via drinking water. **(B)** Representative immunofluo-

rescence images demonstrating the spatial relationship between EdU-positive cells and myofibers. **(C)** Two-week GsMTx4 treatment significantly elevated the proportion of EdU-positive cells beneath the sarcolemma ($n=5$; mean \pm SD; Student's *t*-test). Statistical significance was established at $P < 0.05$. * $P < 0.05$. Scale bar, 50µm

Acknowledgements

Not applicable.

Author contributions

M.L. and N.N.Y. contributed to research design. W.G.W., M.Y.H. and X.S.M. developed the experiment methods and completed all the experiments. K.M. conducted the statistical analysis. N.N.Y. and W.G.W. wrote the original draft, and M.L. revised it. All the authors read and approved the final manuscript.

Funding

This study was sponsored by the Key Research Projects of Colleges and Universities of Henan Province (24A320066); the Medical Science and Technology Project of Henan Province (LHGJ20230198); the National Natural Science Foundation of China (82202767); the Central High-Level Hospital Clinical Research Funding (2022-PUMCH-D-004).

Data availability

No datasets were generated or analysed during the current study.

Declarations

Ethics declarations

This study was approved by the institutional research ethics board. Animal experiments were performed according to protocols approved by the experimental animal welfare ethics committee.

Consent for publication

All authors have read and agreed with the submission of the manuscript. This manuscript has not been published or presented elsewhere in part or in entirety.

Conflict of interest

The author(s) declared no potential conflicts of interest concerning the research, authorship, and/or publication of this article.

Author details

¹Department of Orthopedics, The First Affiliated Hospital of Zhengzhou University, Zhengzhou 450052, China

²Department of Orthopedics, Zhongnan Hospital of Wuhan University, Wuhan 430071, China

³Department of Emergency Medicine, The First Affiliated Hospital of Zhengzhou University, Zhengzhou 450052, China

Received: 28 June 2024 / Accepted: 25 April 2025

Published online: 14 May 2025

References

- Dowling JJ, Wehl CC, Spencer MJ. Molecular and cellular basis of genetically inherited skeletal muscle disorders. *Nat Rev Mol Cell Biol.* 2021;22(11):713–32.
- Birnkrant DJ, et al. Diagnosis and management of Duchenne muscular dystrophy, part 1: diagnosis, and neuromuscular, rehabilitation, endocrine, and Gastrointestinal and nutritional management. *Lancet Neurol.* 2018;17(3):251–67.
- Choi E, Koo T. CRISPR technologies for the treatment of Duchenne muscular dystrophy. *Mol Ther.* 2021;29(11):3179–91.
- Olson E. N 2021 Toward the correction of muscular dystrophy by gene editing. *Proc Natl Acad Sci U S A* 118 22–.
- Lim KR, Maruyama R, Yokota T. Eteplirsen in the treatment of Duchenne muscular dystrophy. *Drug Des Devel Ther.* 2017;11:533–45.
- Duan D, et al. Duchenne muscular dystrophy. *Nat Reviews Disease Primers.* 2021;7(1):13.

7. Guo J, et al. Trends in piezo channel research over the past decade: A bibliometric analysis. *Front Pharmacol*. 2021;12:668714.
8. Jiang Y, et al. Structural designs and mechanogating mechanisms of the mechanosensitive piezo channels. *Trends Biochem Sci*. 2021;46(6):472–88.
9. Ma N, et al. Piezo1 regulates the regenerative capacity of skeletal muscles via orchestration of stem cell morphological States. *Sci Adv*. 2022;8(11):eabn0485.
10. Gnanasambandam R, et al. GsMTx4: mechanism of inhibiting mechanosensitive ion channels. *Biophys J*. 2017;112(1):31–45.
11. Ward CW, et al. GsMTx4-D provides protection to the D2.mdx mouse. *Neuromuscul Disord*. 2018;28(10):868–77.
12. Wang J, et al. GsMTx4-D is a cardioprotectant against myocardial infarction during ischemia and reperfusion. *J Mol Cell Cardiol*. 2016;98:83–94.
13. Suchyna T.M. Piezo channels and GsMTx4: two milestones in our Understanding of excitatory mechanosensitive channels and their role in pathology. *Prog Biophys Mol Biol*. 2017;130(Pt B):244–53.
14. Chemello F, et al. Degenerative and regenerative pathways underlying Duchenne muscular dystrophy revealed by single-nucleus RNA sequencing. *Proc Natl Acad Sci U S A*. 2020;117(47):29691–701.
15. Petrany MJ, et al. Single-nucleus RNA-seq identifies transcriptional heterogeneity in multinucleated skeletal myofibers. *Nat Commun*. 2020;11(1):6374.
16. Motohashi N, Asakura Y, Asakura A. Isolation, culture, and transplantation of muscle satellite cells. *J Vis Exp*, 2014(86).
17. Kottlors M, Kirschner J. Elevated satellite cell number in Duchenne muscular dystrophy. *Cell Tissue Res*. 2010;340(3):541–8.
18. Hawke TJ, Garry DJ. Myogenic satellite cells: physiology to molecular biology. *J Appl Physiol* (1985). 2001;91(2):534–51.
19. Robin G, Berthier C, Allard B. Sarcoplasmic reticulum Ca²⁺ permeation explored from the lumen side in Mdx muscle fibers under voltage control. *J Gen Physiol*. 2012;139(3):209–18.
20. Scripture-Adams DD, et al. Single nuclei transcriptomics of muscle reveals intra-muscular cell dynamics linked to dystrophin loss and rescue. *Commun Biol*. 2022;5(1):989.
21. Hirano K et al. The mechanosensitive ion channel PIEZO1 promotes satellite cell function in muscle regeneration. *Life Sci Alliance*, 2023. 6(2).
22. Ortuste Quiroga HP et al. Fine-Tuning of Piezo1 expression and activity ensures efficient myoblast fusion during skeletal myogenesis. *Cells*, 2022. 11(3).
23. Peng Y, et al. Mechano-signaling via Piezo1 prevents activation and p53-mediated senescence of muscle stem cells. *Redox Biol*. 2022;52:102309.
24. Tsuchiya M, et al. Cell surface flip-flop of phosphatidylserine is critical for PIEZO1-mediated myotube formation. *Nat Commun*. 2018;9(1):2049.
25. Bosutti A, et al. Time window effect of Yoda1-evoked Piezo1 channel activity during mouse skeletal muscle differentiation. *Acta Physiol (Oxf)*. 2021;233(4):e13702.
26. Wang J, et al. Tethering piezo channels to the actin cytoskeleton for mechanogating via the cadherin- β -catenin mechanotransduction complex. *Cell Rep*. 2022;38(6):110342.
27. Cutler AA, et al. The regenerating skeletal muscle niche drives satellite cell return to quiescence. *iScience*. 2022;25(6):104444.
28. Collins BC, et al. Three-dimensional imaging studies in mice identify cellular dynamics of skeletal muscle regeneration. *Dev Cell*. 2024;59(11):1457–e14745.
29. Watt KI, et al. Yap is a novel regulator of C2C12 myogenesis. *Biochem Biophys Res Commun*. 2010;393(4):619–24.
30. Whitehead NP, Yeung EW, Allen DG. Muscle damage in Mdx (dystrophic) mice: role of calcium and reactive oxygen species. *Clin Exp Pharmacol Physiol*. 2006;33(7):657–62.
31. Yeung EW, et al. Effects of stretch-activated channel blockers on [Ca²⁺]_i and muscle damage in the Mdx mouse. *J Physiol*. 2005;562(Pt 2):367–80.
32. Lin BL et al. Pharmacological TRPC6 inhibition improves survival and muscle function in mice with Duchenne muscular dystrophy. *JCI Insight*. 2022;7(19).
33. Burr AR, Molkentin JD. Genetic evidence in the mouse solidifies the calcium hypothesis of myofiber death in muscular dystrophy. *Cell Death Differ*. 2015;22(9):1402–12.
34. Hirata Y, et al. A Piezo1/KLF15/IL-6 axis mediates immobilization-induced muscle atrophy. *J Clin Invest*. 2022;132(10):1–13.
35. Tokumitsu H, Sakagami H. Molecular mechanisms underlying Ca²⁺/Calmodulin-Dependent protein kinase kinase signal transduction. *Int J Mol Sci*. 2022. 23(19).
36. Iwata Y, et al. Dominant-negative Inhibition of Ca²⁺ influx via TRPV2 ameliorates muscular dystrophy in animal models. *Hum Mol Genet*. 2009;18(5):824–34.
37. Gervásio OL, et al. TRPC1 binds to caveolin-3 and is regulated by Src kinase - role in Duchenne muscular dystrophy. *J Cell Sci*. 2008;121(Pt 13):2246–55.
38. Millay DP, et al. Calcium influx is sufficient to induce muscular dystrophy through a TRPC-dependent mechanism. *Proc Natl Acad Sci U S A*. 2009;106(45):19023–8.

Publisher's note

Springer Nature remains neutral with regard to jurisdictional claims in published maps and institutional affiliations.